

# AIFL: A Global Daily Streamflow Forecasting Model Using Deterministic LSTM Pre-trained on ERA5-Land and Fine-tuned on IFS

Maria Luisa Taccari<sup>1</sup>, Kenza Tazi<sup>1</sup>, Oisín M. Morrison<sup>2</sup>, Andreas Grafberger<sup>2</sup>, Juan Colonese<sup>1</sup>, Corentin Carton de Wiart<sup>1</sup>, Christel Prudhomme<sup>1</sup>, Cinzia Mazzetti<sup>1</sup>, Matthew Chantry<sup>1</sup>, and Florian Pappenberger<sup>1</sup>

<sup>1</sup>*European Centre for Medium-Range Weather Forecasts (ECMWF), Reading, United Kingdom*

<sup>2</sup>*European Centre for Medium-Range Weather Forecasts (ECMWF), Bonn, Germany*

February 19, 2026

## Abstract

Reliable global streamflow forecasting is essential for flood preparedness and water resource management, yet data-driven models often suffer from a performance gap when transitioning from historical reanalysis to operational forecast products. This paper introduces AIFL (Artificial Intelligence for Floods), a deterministic LSTM-based model designed for global daily streamflow forecasting. Trained on 18,588 basins curated from the CARAVAN dataset, AIFL utilises a novel two-stage training strategy to bridge the reanalysis-to-forecast domain shift. The model is first pre-trained on 40 years of ERA5-Land reanalysis (1980–2019) to capture robust hydrological processes, then fine-tuned on operational Integrated Forecasting System (IFS) control forecasts (2016–2019) to adapt to the specific error structures and biases of operational numerical weather prediction. To our knowledge, this is the first global model trained end-to-end within the CARAVAN ecosystem. On an independent temporal test set (2021–2024), AIFL achieves high predictive skill with a median modified Kling–Gupta Efficiency (KGE') of 0.66 and a median Nash-Sutcliffe Efficiency (NSE) of 0.53. Benchmarking results show that AIFL is highly competitive with current state-of-the-art global systems, achieving comparable accuracy while maintaining a transparent and reproducible forcing pipeline. The model demonstrates exceptional reliability in extreme-event detection, providing a streamlined and operationally robust baseline for the global hydrological community.

## 1 Introduction

Global-scale streamflow forecasting is a critical capability for disaster risk reduction, supporting humanitarian aid, water resource management, and climate adaptation. The European Centre for Medium-Range Weather Forecasts (ECMWF) has long served as a central hub for these efforts, providing the computational backbone for the Copernicus Emergency Management Service's Global Flood Awareness System (GloFAS) [1]. Historically, hydrological forecasting has relied on a spectrum of approaches ranging from empirical relationships to complex, physically based frameworks [2]. GloFAS traditionally relies on coupling numerical weather predictions (NWP) with process-based hydrological models to generate operational alerts. These models require rigorous calibration to link parameters to global geophysical maps—such as land cover, topography, and soil texture—using in-situ river discharge observations and forcing data like ERA5 [3]. In GloFAS, this process is further enhanced by regionalization methods that transfer

parameters from gauged "donor" catchments to ungauged regions based on geographical and climatic similarity [4]. However, while these process-based models are credible alternatives to in-situ measurements, they face significant challenges in representing complex hydrological processes accurately and are often limited by the quality and spatial resolution of climate-weather forcing variables [3]. These constraints, alongside the high computational demand for global-scale simulations, have motivated increasing interest in data-driven alternatives that can deliver fast, scalable inference while maintaining competitive predictive skill.

The application of machine learning (ML) to Earth system forecasting has recently accelerated, first transforming meteorology. ECMWF is pioneering this shift with the Artificial Intelligence Forecasting System (AIFS), a graph neural network-based model that now competes with physics-based NWP in medium-range accuracy [5]. As detailed by Moldovan et al. [6], AIFS has transitioned to fully operational status and is expanding its capabilities beyond atmospheric variables to include land-surface outputs such as runoff, signalling a convergence of meteorological and hydrological ML capabilities.

A similar paradigm shift has occurred in hydrology [7]. Kratzert et al. [8] argued that ML models typically outperform traditional approaches when trained on large, diverse datasets rather than single basins. This hypothesis has been validated by the widespread adoption of Long Short-Term Memory (LSTM) networks, which have demonstrated the ability to learn universal hydrological behaviours, outperforming regionally calibrated process-based models and enabling accurate prediction in ungauged basins [9]. This success has spurred a diverse family of advanced architectures, such as Hydra-LSTM [10], which employs a semi-shared architecture to improve multi-basin prediction, and MC-LSTM [11], which integrates mass conservation constraints directly into the network structure.

Most state-of-the-art approaches employ a lumped formulation [12], where the LSTM operates on inputs spatially aggregated over the entire catchment, including both time-varying meteorological forcings and static attributes such as topography, soil properties, and land cover. By collapsing the spatial distribution of these features into basin-wide aggregates, these models inherently overlook sub-catchment heterogeneity and the internal dynamics of lateral water routing. This structural simplification limits the utility of such models for tasks requiring fine-scale flow propagation or the representation of discrete hydrological features such as lakes, dams, and barrages [13].

To bridge this gap, a new generation of spatially explicit architectures has emerged. These range from implicit routing methods that learn flow propagation end-to-end [14, 15] to explicit hybrid frameworks that combine ML-based runoff generation with physically inspired transport schemes [16–18]. For instance, the DROP (Deep Runoff Prediction and propagation) framework [19] addresses these structural limitations by coupling drainage-unit scale LSTMs with an explicit routing module, allowing for a more transparent and physically interpretable modulation of flow. However, the path to global implementation remains uneven; while some hybrid methods offer high fidelity, they often entail substantial computational overhead or rely on detailed river connectivity data that is not yet globally available. Consequently, deploying these spatially resolved methods in real-time operational systems remains a significant technical challenge.

New global forecasting capabilities have emerged from these data-driven advances. Google's global flood forecasting model established a high benchmark for reliability in ungauged watersheds [20] using a specialized hindcast-forecast architecture. However, a critical operational gap remains for the broader research community: the mismatch between training data (historical reanalysis) and inference data (operational forecasts). Standardised datasets like CAMELS [21] and CARAVAN [22] predominantly rely on meteorological reanalysis data (e.g., ERA5). Operational forecasting requires driving models with NWP forecasts, such as the ECMWF Integrated Forecasting System (IFS), which exhibit different error structures. This distribution shift often leads to degraded operational performance when models trained on "perfect" reanalysis are exposed to real-time forecast noise [23]. Addressing this challenge, Konold et al. [24] demonstrated

that a "domain shift" occurs when transitioning from reanalysis to forecast products, resulting in a significant reduction in predictive skill if not explicitly mitigated.

Importantly, this limitation is orthogonal to architectural complexity. Even state-of-the-art models—whether spatially aggregated (lumped), connectivity-aware (graph-based), or those integrating physical constraints and process-based structures (hybrid)—are fundamentally constrained by the characteristics of their forcing data. Addressing this reanalysis-to-forecast domain shift is therefore a prerequisite for reliable operational deployment. Leveraging the recently introduced CARAVAN MultiMet dataset [25], we introduce AIFL (Artificial Intelligence for Floods). Unlike previous works that utilise complex probabilistic or explicit graph-based connectivity, AIFL utilises a standard, deterministic LSTM architecture trained on the entire CARAVAN dataset (over 18,000 basins) to provide a scalable baseline.

The primary contribution of AIFL is a novel two-stage training strategy designed to solve the reanalysis-to-forecast domain shift. Inspired by findings that fine-tuning pre-trained models improves generalisation [26], we apply this concept to the temporal and data-source domain. We first pretrain the model on 40 years of ERA5-Land reanalysis to learn robust physical processes, and then fine-tune it on IFS control forecasts to adapt to operational biases. This approach offers a transparent, reproducible baseline for global operational flood forecasting.

The remainder of this paper is organized as follows: Section 2 details the data curation process; Section 3 describes the model architecture and the two-stage training strategy; Section 4 evaluates the model's predictive skill; and Section 5 concludes with future directions.

## 2 Data Curation & Experimental Design

This section describes the data sources and processing steps, used to develop the AIFL model. The focus is on constructing a globally consistent, non-redundant training set that supports a two-stage reanalysis-to-forecast learning strategy. The AIFL framework (shown in Figure 1 and detailed further in Section 3) utilises separate feedforward embedding networks to process static landscape attributes and dynamic meteorological forcings. These inputs are integrated by an LSTM core to produce streamflow forecasts; this architecture necessitates the specific data curation steps outlined below.

### 2.1 Datasets and Target Variable

The model is trained to predict daily streamflow in the form of specific discharge ( $\text{mm d}^{-1}$ ), utilizing station-based observations from the CARAVAN dataset v1.5 [22] and its extensions. Specific discharge—defined as discharge normalised by the catchment drainage area—simplifies the learning task by aligning the units of the target variable with meteorological inputs such as precipitation. This design choice avoids the network learning linear basin-area scaling through complex transformations, while still incorporating basin size as an explicit input through the static attributes to capture mechanisms such as basin capacity or lag time.

### 2.2 Deduplication and Quality Control

The raw CARAVAN dataset initially includes 22,371 basins. Because CARAVAN aggregates data from multiple independent providers—including the Hydrometeorological Sandbox of École de technologie supérieure (HYSETS) [27], the Catchment Attributes and Meteorology for Large-sample Studies (CAMELS) dataset [28], and the GRDC-Caravan extension [29] which integrates data from the Global Runoff Data Centre (GRDC)—it lacks a unified quality-control standard and inherently contains spatial overlaps among its constituent datasets. In global hydrological archives, stations frequently represent nested catchments or identical physical locations reported under different identifiers. Retaining such stations without filtering leads to information leakage and artificially inflated model performance. In addition, when two stations exhibit substantial

## AIFL: GLOBAL LSTM-BASED STREAMFLOW FORECASTING FRAMEWORK

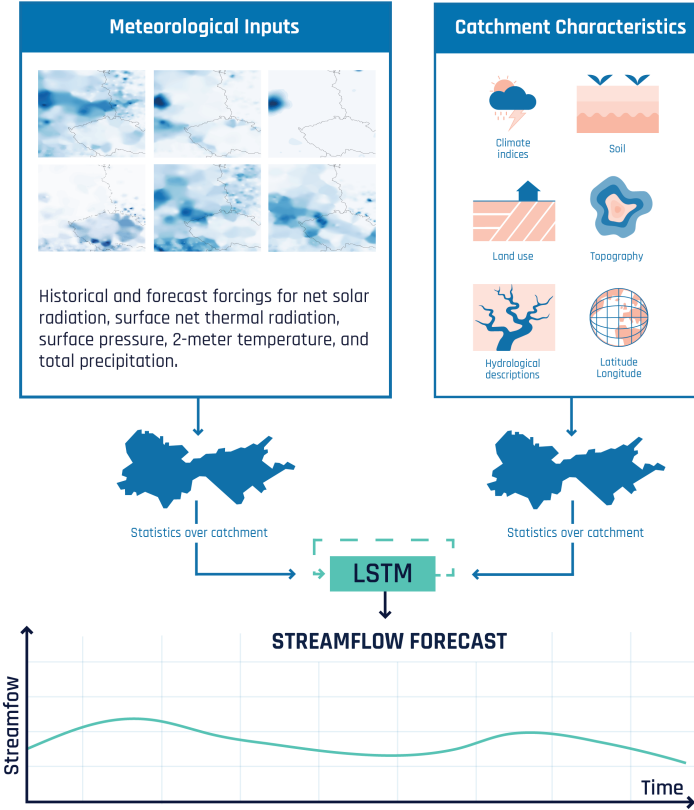


Figure 1: Schematic of the AIFL framework. The model architecture uses separate Multi-Layer Perceptron (MLP) embedding layers for static and dynamic inputs, feeding a shared LSTM core that processes a 170-day hindcast-window to generate 10-day forecasts. The training strategy transitions from ERA5-Land reanalysis pre-training to IFS forecast fine-tuning to resolve domain shifts.

spatial overlap but provide conflicting discharge records, a data-driven model cannot reconcile the two signals consistently and instead learns an interpolated behaviour that does not accurately represent either catchment.

To address this issue, a systematic deduplication and quality-control procedure is applied based on basin geometry and observed discharge similarity. Basin boundaries are taken directly from the original catchment polygon shapefiles provided by each source dataset and are reprojected to a common geographic coordinate system (EPSG:4326). Spatial overlap is computed purely at the vector polygon level, without reference to gridded products or model resolution. For each basin polygon, its area is compared against all candidate polygons, and the fractional overlap is defined as the intersecting area normalised by the smaller of the two basin areas. Basin pairs with a fractional overlap greater than or equal to 0.7 are flagged for further inspection.

For each flagged pair, the Kling–Gupta Efficiency (KGE) [30] is computed between the corresponding observed streamflow time series. Pairs with  $KGE \geq 0.95$  are classified as strict duplicates, and 2,007 stations are removed from the training set. Among duplicate pairs, stations with the longest observational records after 2016 are preferentially retained in order to maximize overlap with the availability of high-resolution operational forcing data. Determinis-

tic IFS forecasts at approximately  $0.1^\circ$  horizontal resolution become available in March 2016 with the implementation of Cycle 41r2 [31] and provide the high-fidelity inputs required for model fine-tuning and inference. Basin pairs with poor agreement ( $\text{KGE} < 0.6$ ) are discarded entirely, as such discrepancies likely indicate data quality issues. Intermediate cases ( $0.6 \leq \text{KGE} < 0.95$ ) are retained, as they typically correspond to genuinely distinct hydrological behaviour in nested sub-catchments.

After an additional quality-control step that removes implausible or severely discontinuous discharge time series, a final curated set of 18,588 unique basins remains. In particular, non-physical or erroneous signals are identified using a flatline ratio, defined as the proportion of invariant consecutive observations computed for each station. Basins exhibiting high flatline ratios or near-zero variance are excluded. The global spatial distribution of the resulting basins is shown in Figure 2.

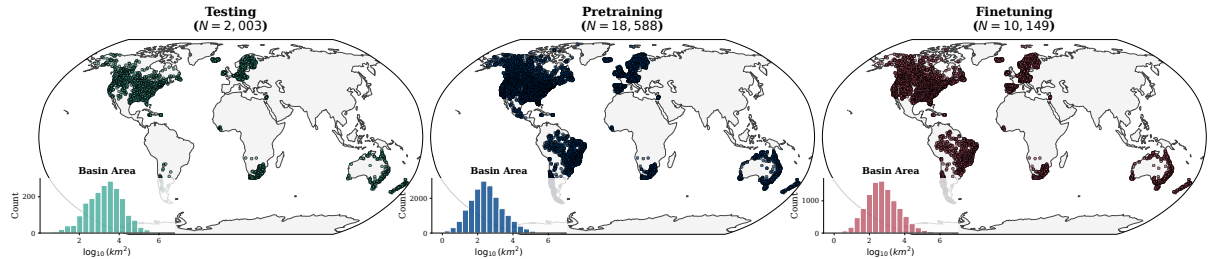


Figure 2: Global spatial distribution of the 18,588 quality-controlled streamflow stations across the three experimental stages: pre-training, fine-tuning, and testing. The inset diagrams provide the frequency distribution of basin surface areas (on a  $\log_{10}$  scale) for each subset.

### 2.3 Model Inputs and Consistency

The model relies on two types of inputs: dynamic features, which vary over time, and static features, which remain constant for each catchment. Dynamic features include the five core meteorological drivers: surface net solar radiation (SSR), surface net thermal radiation (STR), surface pressure (SP), 2-m air temperature (T2M), and total precipitation (TP)—as summarized in Table 1. Static features consist of 203 catchment attributes describing physiography, soil properties, geology, land cover, climatology, and anthropogenic influence. These feature types are processed separately through dedicated embedding networks before being integrated into the LSTM core.

Table 1: Input features for the AIFL model. The selection is restricted to variables shared across ERA5-Land reanalysis and IFS forecasts in the CARAVAN MultiMet dataset [25] to facilitate seamless transferability from pre-training to operational inference.

Variable	Description	Unit
SSR	Surface net solar radiation	$\text{W m}^{-2}$
STR	Surface net thermal radiation	$\text{W m}^{-2}$
SP	Surface pressure	kPa
T2M	Air temperature at 2 metres	°C
TP	Total daily precipitation	$\text{mm d}^{-1}$

While incorporating additional predictors, higher temporal resolution, or more descriptive spatial aggregations (e.g., basin-scale maxima, variability, or other statistics rather than simple catchment-averaged means) would likely improve performance, AIFL is currently constrained to

this standardised daily input set. These variables are provided consistently across both ERA5-Land reanalysis and operational IFS forecasts through the CARAVAN MultiMet extension [25], ensuring that the input space remains identical between pre-training and operational fine-tuning.

The static catchment attributes are sourced from the CARAVAN dataset [22], which offers a globally consistent description of landscape characteristics governing hydrological response. These features, primarily aggregated from HydroATLAS [32], encompass diverse environmental categories. They describe the physical structure of the basin through metrics such as mean elevation and slope, the subsurface environment via soil texture and lithology, and the surface conditions through vegetation indices and land-use fractions. Climatological indices representing long-term averages and anthropogenic descriptors, such as population density and degree of regulation, are also included to allow the model to distinguish between different hydrological regimes.

Beyond the original CARAVAN attributes, additional time-aware features are introduced to improve temporal representation. Seasonal information is encoded using sine and cosine transformations of day-of-year and month. In addition, each station’s Coordinated Universal Time (UTC) offset is provided as an explicit input to facilitate correct temporal alignment between UTC-based meteorological forcings and local-time streamflow observations. We deliberately avoid a direct conversion of streamflow time series to UTC, as the required temporal interpolation would introduce non-physical artifacts and potentially degrade the integrity of the original peak-flow observations. By providing the UTC offset as a static attribute, we allow the LSTM core to learn the necessary phase shifts between forcing and response without altering the raw observational data.

## 2.4 Data Availability for Temporal Evaluation

This study focuses on temporal generalisation, evaluating the model’s ability to forecast future events at established gauging stations. While spatial extrapolation to ungauged basins remains a critical challenge, the present experimental design specifically targets an operational forecasting setting where predictions are issued for fixed, historically observed locations. We therefore utilise the full set of stations as a consistent reference for the pre-training, fine-tuning and testing phases, ensuring the model captures a global diversity of hydrological signatures.

The decision to maintain a consistent set of gauging stations, rather than implementing a spatial split, is driven primarily by data availability. As shown in Figure 3, there is a sharp decline in active station records after 2015, as many constituent datasets within the CARAVAN framework lack updates beyond 2018–2019. Partitioning the remaining active stations for both spatial and temporal validation would yield a test set for the 2021–2024 period that is too small to be climatically or geographically representative.

For the independent temporal test period (2021–2024), we identified a subset of 2,003 basins where continuous streamflow observations remained available during the operational forcing window. While the overall dataset spans a consistent range of spatial scales—from small headwater catchments (approximately  $1 \text{ km}^2$ ) to continental-scale river systems exceeding  $10^6 \text{ km}^2$ —the subset of basins available for evaluation during the operational testing period is skewed toward larger catchments. This shift reflects the availability of streamflow gauge records that overlap with the operational forcing period and results in model evaluation being concentrated on larger river systems. Despite this inherent weighting, the 2,003-station subset maintains sufficient hydroclimatic diversity to provide a robust assessment of model performance under strictly future meteorological conditions. While developing strategies to better leverage the sparse records available for operational testing—and balancing evaluation across all spatial scales—remains a critical frontier for global hydrology, such methodological refinements are reserved for future work.

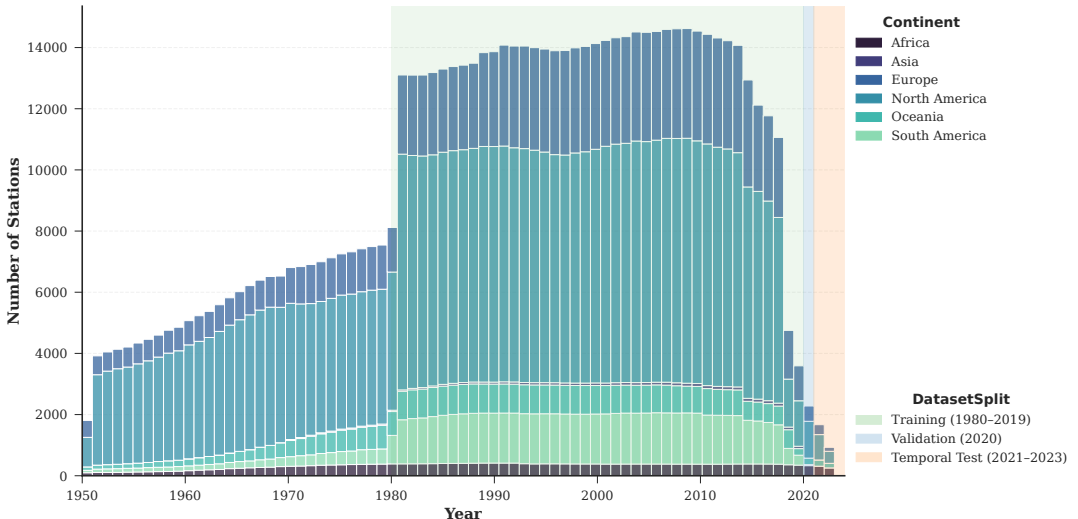


Figure 3: Global station availability over time (1950–2023). Shaded regions indicate the splits for pre-training and fine-tuning (green), validation (blue), and testing (orange).

### 3 Methodology

This section describes the architecture and training strategy of the AIFL model. The model is implemented using the open-source NeuralHydrology framework [33] as a starting point. While the core LSTM architecture follows NeuralHydrology’s implementation, we introduce several extensions and adaptations—particularly in data preprocessing, training configuration, and forecast-time inference—to support global-scale pre-training on ERA5-Land and subsequent fine-tuning with IFS operational forecasts. The methodology is designed to learn physically meaningful rainfall-runoff relationships from reanalysis data while enabling robust adaptation to operational numerical weather prediction forcings.

#### 3.1 Model Architecture

The AIFL model employs a single-layer LSTM network to capture temporal rainfall-runoff dynamics across a 180-day window. This duration was chosen via sensitivity analysis to balance hydrological memory with computational efficiency; extending the window to 365 days (as seen in [20]) yielded negligible accuracy gains while significantly increasing training overhead. To handle high-dimensional inputs, dynamic features and static features are first transformed through separate three-layer feedforward embedding networks (layer sizes 30, 20, 64) with tanh activation functions. The embeddings are then concatenated and fed into the LSTM to produce 10-day output sequences. The architectural specifications are summarized in Table 2.

This configuration was selected based on early architectural development that evaluated generalisation performance across both temporal and spatial settings. Although the operational focus of AIFL is temporal forecasting, spatial validation was utilised to assess whether the model could learn robust physical representations of hydrological heterogeneity.

While no systematic hyperparameter search was performed, a 1,024-unit model and a smaller 256-unit model, proposed by Ryd and Nearing [26], were compared. While both architectures showed comparable skill in temporal test sets, the 1,024-unit model demonstrated significantly higher representational capacity in spatial generalisation, achieving a median NSE of 0.63 compared to 0.48 for the smaller model. These results indicate that a larger hidden state is essential for capturing the global variability of hydrological signatures, justifying the selection of the 1,024-unit architecture for all subsequent training and fine-tuning phases.

Table 2: Summary of the AIFL model architecture and hyperparameter choices.

Component	Configuration
Recurrent layer	Single-layer LSTM
Hidden state size	1024
Dropout (output)	0.4
Static embedding	3-layer MLP (30, 20, 64) with tanh
Dynamic embedding	3-layer MLP (30, 20, 64) with tanh
Temporal window	180 days
Output sequence length	10 days
Input features	5 dynamic variables + 203 static attributes

### 3.2 Training Strategy

The model is trained using a normalised Mean Squared Error (MSE) loss function following [34], which ensures that all basins contribute equally to the optimization process regardless of their absolute flow magnitude:

$$\mathcal{L}_{\text{norm-MSE}} = \frac{1}{N} \sum_{i=1}^N \left( \frac{(y_i - \hat{y}_i)^2}{\sigma_{\text{basin}(i)}^2 + \varepsilon} \right), \quad (1)$$

where  $y_i$  and  $\hat{y}_i$  denote observed and predicted specific discharge, and  $\sigma_{\text{basin}(i)}$  is the standard deviation of the observed discharge for the corresponding basin calculated over the training period. The constant  $\varepsilon = 0.1$  is added for numerical stability to prevent division by very small variances, and  $N$  is the total number of training samples (time steps across all basins) in the current training batch. This local normalisation of the loss function ensures that the model is not biased toward basins with high-flow variability. All dynamic and static input features are z-score normalised on a per-variable basis using global training statistics before being fed into the embedding networks.

Systematic distributional shifts exist between the ERA5-Land reanalysis used during model development and the operational IFS forcings encountered in real-time forecasting. To accommodate these discrepancies between historical training data and operational environments, we adopt a two-stage transfer learning strategy that transitions from reanalysis-driven pre-training to forecast-aligned fine-tuning. Unlike the coupled data assimilation used in operational IFS streams, ERA5-Land is produced as an offline land-surface "replay" with specific elevation corrections for thermodynamic states, resulting in a distinct statistical signature [35]. As illustrated by the normalised Wasserstein distance in Figure 4, discrepancies between ERA5-Land and operational IFS precipitation can be substantial across large parts of the globe. Without an explicit alignment phase, a model trained solely on reanalysis would propagate these forcing inconsistencies directly into its streamflow simulations, leading to degraded performance in real-time deployment. Our strategy resolves this by first utilizing the multi-decadal, physically consistent ERA5-Land record (1980–2019) to learn universal hydrological response functions, before subsequently fine-tuning all model weights on IFS control forecasts (2016–2019). This second stage allows the LSTM to adapt its internal representations to the specific error structures and statistical characteristics of the operational NWP stream, effectively correcting for forecast-induced biases like those observed in the Hokitika River example (Figure 5).

In the pre-training phase, the network is optimised on ERA5-Land reanalysis inputs using 180-day sequences spanning 1 January 1980 to 31 December 2019 across all 18,588 basins (Table 3). The objective of this phase is to learn general, physically meaningful rainfall–runoff relationships from a long and internally consistent historical record. Training uses the Adam optimizer with an initial learning rate of  $4 \times 10^{-4}$ , gradient clipping at 1.0, and Gaussian target

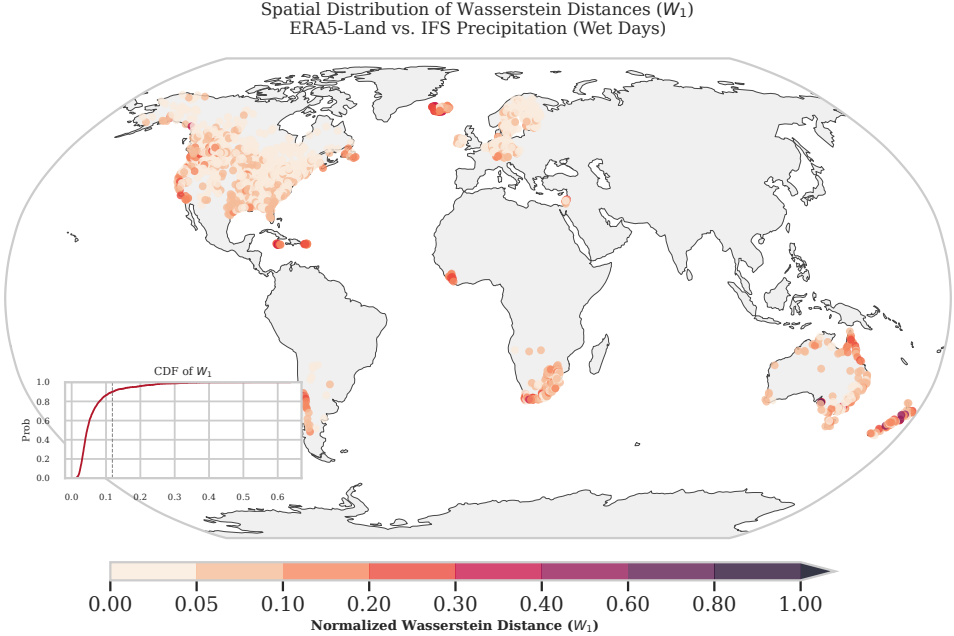


Figure 4: Global spatial distribution of the normalised Wasserstein distance ( $W_1$ ) between ERA5-Land reanalysis and 1-day lead time (LT1) IFS daily precipitation. The metric quantifies the distributional shift between the pre-training and operational forcing data, calculated over a common 4-year period (2016–2019,  $n = 1,461$  days) for 2,003 basins. To ensure cross-climatological comparability,  $W_1$  is computed using only wet days ( $> 1$  mm) and normalised by the mean ERA5-Land wet-day precipitation. The inset Cumulative Distribution Function (CDF) highlights the right-skewed nature of the discrepancies: while the median shift is relatively small (0.045), a “large” difference—defined as the upper decile of the distribution—corresponds to  $W_1 > 0.119$ , with extreme cases reaching 0.638. These high-distance regions identify where operational forecasts deviate most significantly from the training reanalysis, providing a quantitative basis for the necessity of the fine-tuning stage to mitigate forecast-induced streamflow biases.

noise ( $\sigma = 0.02$ ) to improve robustness. A cosine annealing learning-rate schedule is applied over 100 epochs, including 10 warm-up epochs. Each epoch is capped at 10,000 parameter updates with a batch size of 512. Validation is performed every 10 epochs on a fixed subset of 1,000 basins to monitor convergence and prevent overfitting.

Following pre-training, the model is fine-tuned using IFS control forecasts with a 1-day lead time (LT1) over the 2016–2019 period. This second phase explicitly aligns the learned hydrological representation with the statistical properties and systematic biases of the operational forcing. We specifically utilise LT1 for fine-tuning and validation as it provides the most direct representation of the operational IFS data distribution while minimizing the compounding atmospheric errors associated with longer lead times. By aligning the model with the physics and resolution of the LT1 stream, we establish a robust baseline for operational performance; while the operational system extends to a 10-day horizon, the primary objective of this stage is to correct for the fundamental reanalysis-to-forecast shift rather than lead-time-specific drift, which is reserved for future analyses.

To ensure numerical continuity, the ERA5-Land-based input scaler is reused and applied to IFS variables through a one-to-one variable mapping. All model parameters remain unfrozen, allowing the network to adapt its internal representations to forecast-specific error structures. fine-tuning uses the same sequence length and prediction horizon as pre-training, but with a reduced initial learning rate of  $1 \times 10^{-4}$  over 30 epochs and five warm-up epochs. This lower

learning rate limits catastrophic forgetting of the physical relationships learned during pre-training while providing sufficient flexibility to correct forecast-induced biases.

Table 3: AIFL experimental design and operational periods across the 18,588-station network.

Phase	Input Data Source	Period	Primary Purpose
pre-training	ERA5-Land Reanalysis	1980 – 2019	Learn universal hydrology
fine-tuning	IFS Control (LT1)	2016 – 2019	Operational alignment
Validation	IFS Control (LT1)	2020	In-time generalisation
Temporal Test	IFS Control (LT1)	2021 – 2024	Operational performance

The transition from reanalysis-driven pre-training to forecast-aligned fine-tuning substantially reshapes the performance distribution across the 2,003 basins in the temporal test set. While the medians remain largely stable—with a median  $\Delta\text{KGE}'$  (the modified Kling–Gupta Efficiency; [36]) of  $-0.013$  and a median  $\Delta\text{NSE}$  of  $-0.032$ —the two-stage training strategy leads to a pronounced improvement in mean global skill. Specifically, the mean  $\text{KGE}'$  increases from  $0.21$  to  $0.44$ , while the mean  $\text{NSE}$  improves from  $-11.40$  to  $-3.26$ .

The divergence between median and mean changes indicates that fine-tuning primarily improves previously low-performing basins, contracting the lower tail of the performance distribution where the pre-trained model fails to generalise to operational forcings. Overall,  $\text{KGE}'$  improves in 44.7% of basins, with 17.7% of the full sample exhibiting gains exceeding 0.1. Figure 5 illustrates this corrective behaviour in the Hokitika River basin. The pre-trained model exhibits a persistent positive bias, consistently overestimating baseflow and recession levels compared to observations. Fine-tuning effectively corrects this systematic volume error to better align with observed discharge.

The response to fine-tuning is spatially non-uniform. While 22.7% of basins experience notable declines in performance ( $\Delta\text{KGE}' < -0.1$ , defined as the change in  $\text{KGE}'$  between the fine-tuned and pre-trained models), these are outweighed by improvements in previously poorly performing catchments, where the mean increase in  $\text{KGE}'$  among significantly improved basins is 1.75.

This asymmetry confirms that fine-tuning acts primarily as an operational stabilizer: it mitigates severe forecast-induced errors at the cost of minor degradations in already well-calibrated basins. Together, these results motivate the explicit separation between physics-consistent pre-training on reanalysis data and forecast-aligned fine-tuning as a practical strategy for managing distributional drift between reanalysis and operational meteorological forcing streams.

During operational inference, the LT1 forcings are replaced with increasing lead times (1 to 9 days). Results for this setting are shown in Sections 4.2 and 4.3.

## 4 Results and Evaluation

This section evaluates the predictive skill of the AIFL model with a focus on temporal generalisation, operational flood forecasting performance, and comparison against current global benchmarks. All results are reported for a strictly temporal test setting, assessing the model’s ability to forecast future conditions at previously observed gauging locations.

### 4.1 Temporal generalisation and Global Performance

AIFL is evaluated over an independent temporal test period spanning 1 January 2021 to 30 September 2024 at 2,003 gauged basins for which continuous streamflow observations are available during the operational forcing period. Model predictions are compared against observed daily streamflow to assess predictive skill at known locations under operational conditions. The

## HOKITIKA RIVER, GORGE (New Zealand) | Area: 363 km<sup>2</sup>

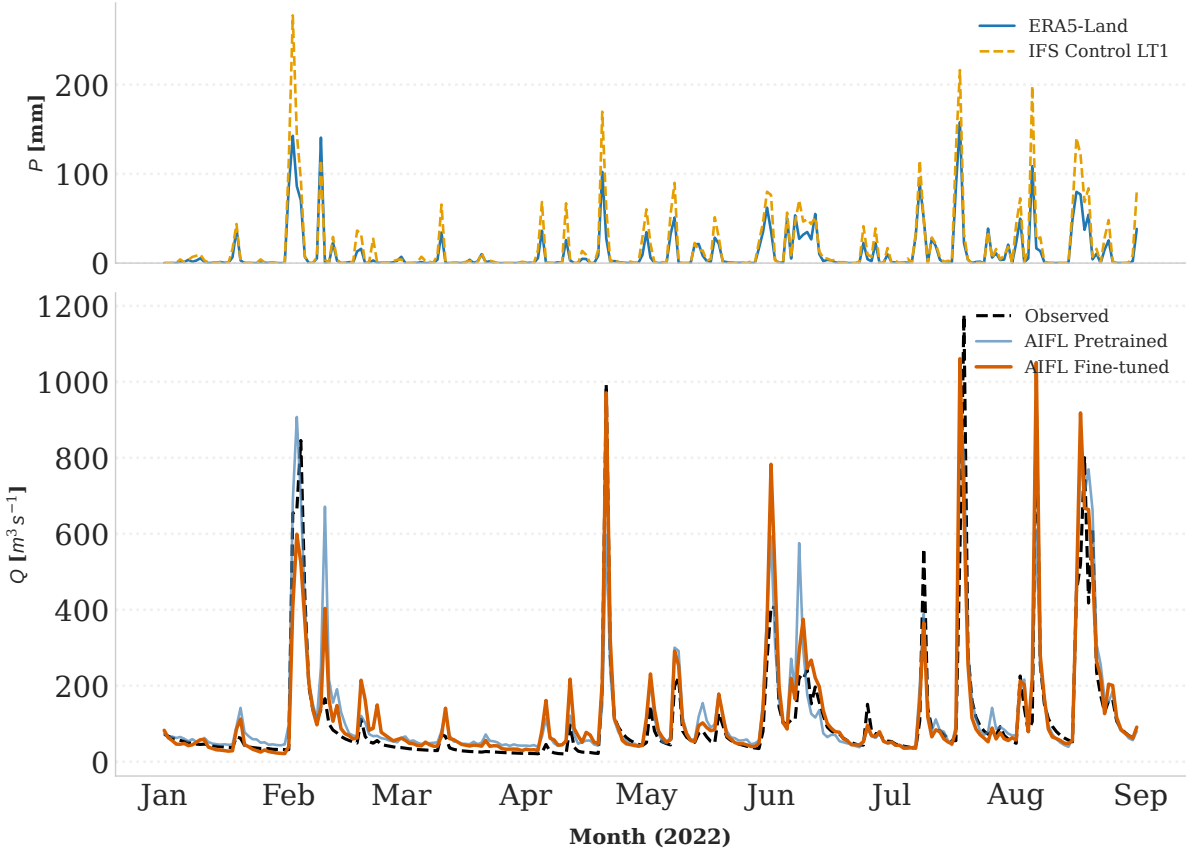


Figure 5: Hydro-meteorological time series for the Hokitika River, Gorge (New Zealand; 363 km<sup>2</sup>) during 2022. Top: precipitation ( $P$ ) from ERA5-Land (blue) and IFS Control LT1 (yellow). Bottom: observed discharge ( $Q$ ; black dashed) compared against two AIFL model configurations both forced by the same IFS Control LT1 inputs: the pre-trained model (steel blue) and the fine-tuned model (red). This direct comparison isolates the impact of the model weights, demonstrating how the fine-tuned AIFL learns to correct for the systematic wet bias in IFS precipitation peaks to align streamflow magnitudes with observations.

test basins represent a geographically diverse subset of the curated dataset and were selected solely based on the availability of observations overlapping with the operational IFS forecast period, rather than through spatial sampling, as detailed in Section 2.4.

All results reported in this section correspond to forecasts driven by IFS Control precipitation at LT1, which serves as a proxy for near-real-time operational forcing while isolating hydrological model skill under operational inputs. Across the test basins, AIFL achieves a median KGE' of 0.66, which exceeds the “satisfactory” performance threshold of 0.50 established in hydrological literature [37]. For context, the GloFAS v4 operational system reports a median KGE' of 0.70 for its 1,995 calibrated stations when evaluated against ERA5-forced reanalysis [38]. A detailed performance comparison between AIFL and the Google global flood model [20], conducted across a shared subset of gauging stations, is provided in Section 4.3.

The observed skill reflects the model’s ability to reproduce streamflow dynamics accurately while correcting for systematic biases in the forcing data. The model maintains a high median Pearson correlation ( $r = 0.81$ ), demonstrating that the LSTM reliably captures the timing and temporal structure of streamflow, while the two-stage fine-tuning strategy mitigates the systematic “wet” bias typical of raw operational forecasts, achieving a median bias ratio ( $\beta$ ) of 1.00 and

near-perfect volume conservation across the global test network. Metric decomposition (Figure 6) confirms that these improvements arise from a combination of strong temporal agreement and neutralization of systematic forcing errors. With a median NSE of 0.53, the model surpasses established “satisfactory” thresholds [39], demonstrating that AIFL generalises robustly to future periods at gauged locations while producing physically consistent and operationally reliable streamflow predictions.

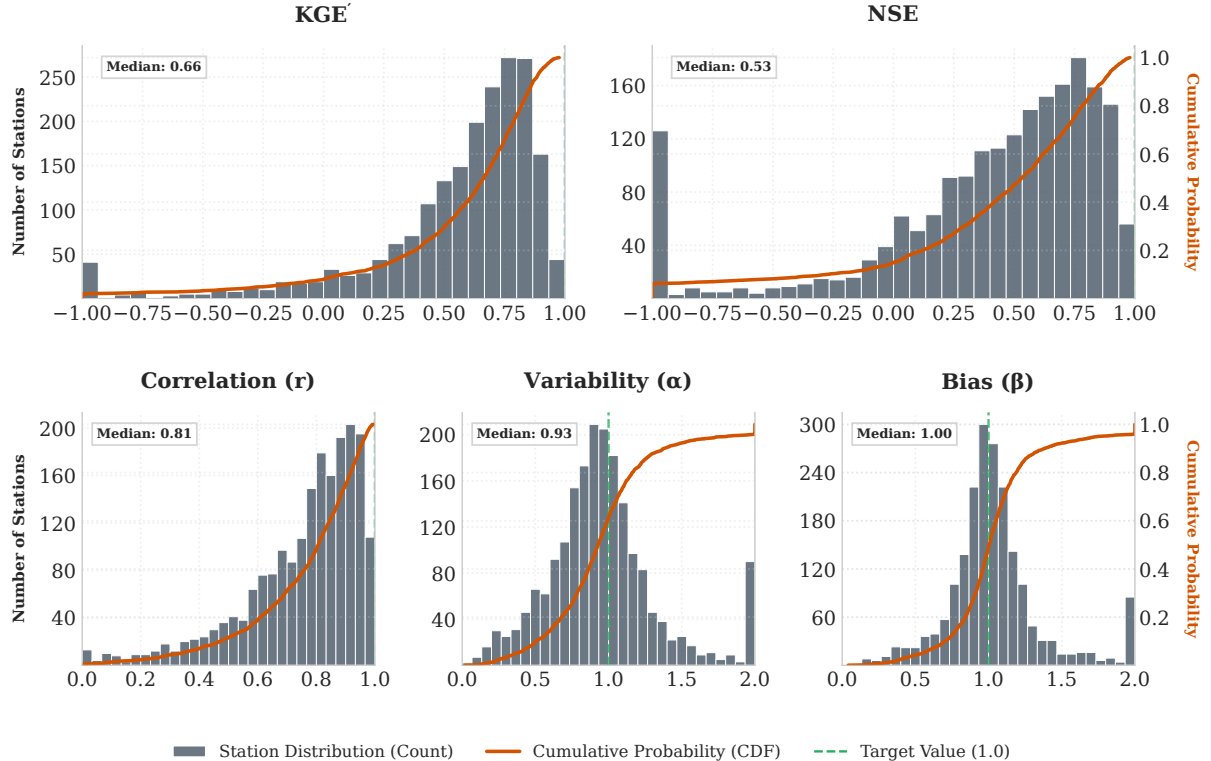


Figure 6: Global performance metrics for the AIFL model across the 2,003 test basins (Section 2.4). Histograms (grey bars) represent the frequency distribution of stations and empirical cumulative distributions (orange) illustrate station-wise results. Green dashed lines denote ideal values (1.0); median values are indicated for each panel.

The spatial distribution of  $\text{KGE}'$  values is shown in Figure 7. Skill is consistently high across Europe, North America, and Oceania, with most basins achieving  $\text{KGE}' > 0.6$ . Lower performance is concentrated in arid and semi-arid regions and in basins characterised by highly-intermittent flow regimes. These catchments typically exhibit long periods of near-zero discharge punctuated by sparse, sharp peaks, which strongly penalize composite performance metrics such as  $\text{KGE}'$ .

## 4.2 Flood Event Performance

Beyond overall temporal accuracy, operational flood forecasting critically depends on the reliable detection of high-flow events. To evaluate this, we define flood events relative to return-period thresholds derived from a long-term reference simulation. Specifically, the AIFL model is driven by ERA5-Land inputs over 1980–2024 to generate multi-decadal simulated discharge time series for each basin. Annual maxima extracted from these simulations are used to estimate return-period thresholds ranging from 1.5 to 50 years using a standard extreme-value framework. While the framework can theoretically produce higher-magnitude estimates, we limit our analysis to a 50-year maximum to ensure statistical robustness. These thresholds are derived by fitting a Gumbel distribution using the first two L-moments ( $\lambda_1, \lambda_2$ ) to provide stable estimates of the

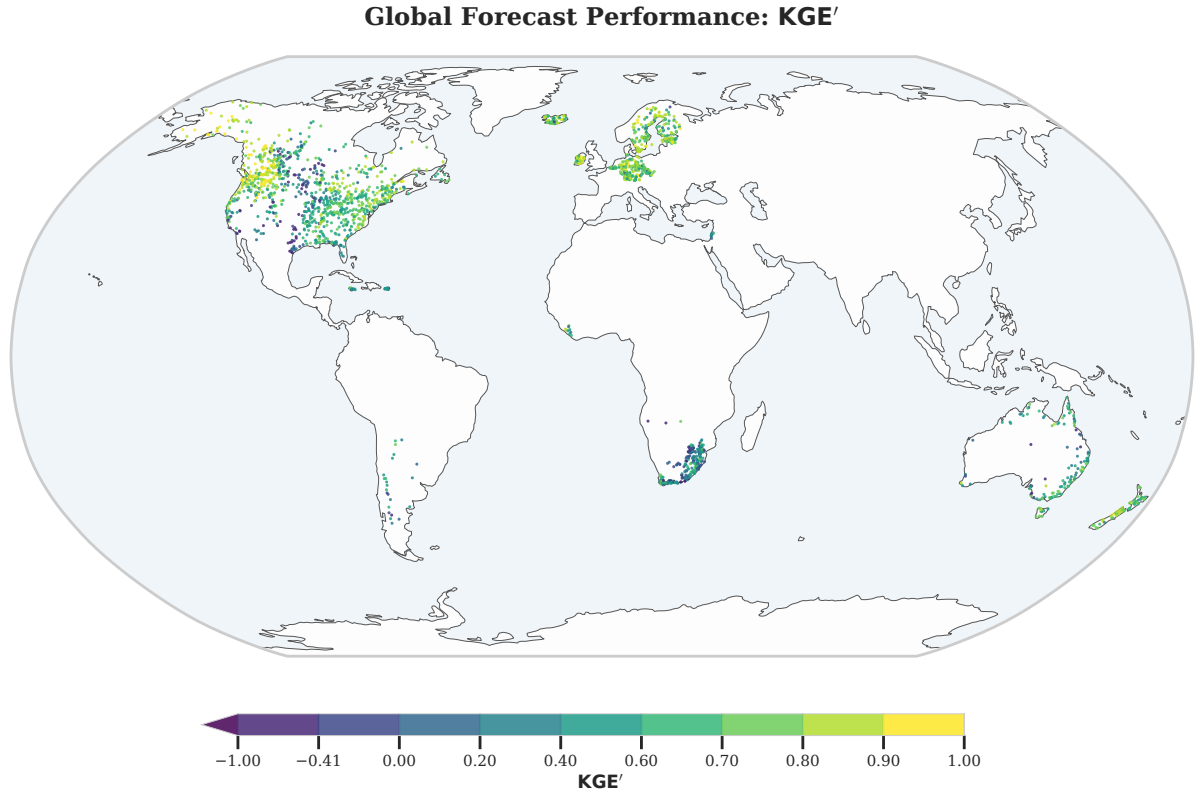


Figure 7: Global map of temporal generalisation performance (KGE') for the 2021–2024 test period. Values above 0.5 are typically considered skillful.

distribution’s location and scale parameters. Defining thresholds in simulated discharge space ensures statistical consistency with the model outputs and avoids biases that would arise from applying observational thresholds, particularly in regions with sparse or uncertain discharge records. To maintain this consistency during evaluation, we adopt a dual-threshold framework: AIFL forecast events are defined by exceedances of thresholds derived from the 45-year (1980–2024) ERA5-Land historical simulation, while observed events are identified when gauge discharge exceeds thresholds derived from the corresponding historical observational record. This utilization of the full climatological record maximizes the sample size of the annual maxima series, providing more stable Gumbel distribution parameters for return periods up to 50 years.

Flood event performance is quantified using precision and recall. Precision measures the fraction of predicted flood events that coincide with observed threshold exceedances on the same day, reflecting the model’s false-alarm behaviour. Recall quantifies the fraction of observed flood events that are successfully identified, indicating sensitivity to true extremes. These metrics are computed exclusively for the predefined test basins under a strict zero-day timing criterion.

When evaluated using exact day-to-day event matching, the AIFL model displays a strongly conservative event-detection behaviour (Table 4). Across all return periods, global precision is equal to 1.0, meaning that every predicted flood exceedance corresponds to an observed event occurring on the same day and that no false alarms are produced. Such behaviour indicates that AIFL triggers flood alerts only under clear hydrological signal conditions, a property that is particularly important for operational early-warning systems where false positives can lead to loss of user trust and unnecessary mobilization of personnel and limited emergency resources [40, 41].

This high reliability is accompanied by a limited but systematic recall. For frequent events (1.5–2-year return periods), the model captures approximately half of all observed exceedances (global recall of 0.54 and 0.51, respectively). Recall decreases progressively with event rarity,

Table 4: Global event-based verification statistics for AIFL under a strict temporal evaluation (margin of error = 0 days). Precision is 1.0 for all return periods, indicating zero false alarms.

Return period (years)	Hits	Misses	False alarms	Global recall
1.5	1,757,086	1,513,494	0	0.54
2.0	859,787	832,195	0	0.51
5.0	176,888	230,671	0	0.43
10.0	64,145	98,589	0	0.39
20.0	25,070	44,267	0	0.36
50.0	8,391	18,054	0	0.32

reaching 0.32 for 50-year floods, reflecting an increasing number of missed extremes. These results indicate that AIFL prioritizes precision over sensitivity, effectively filtering marginal or uncertain events while retaining robust detection of the strongest signals. Improving recall for rare extremes without compromising the current zero-false-alarm behaviour remains an important direction for future development.

While these aggregate statistics summarize global test-set performance, they do not fully convey operational realism during individual extreme events. To illustrate model behaviour in a real-world setting, performance is further examined through a focused case study of the January 2024 floods in Belgium associated with Storm Henk. Figure 8 presents results for the Straintmont station (GRDC ID 6221570) which drains a  $182 \text{ km}^2$  catchment and experienced an approximately 1-in-20-year flood. The model consistently predicts a clear flood signal up to six days in advance of the observed peak discharge. Early forecasts indicate peak magnitudes of approximately  $50 \text{ m}^3 \text{ s}^{-1}$  compared to an observed peak near  $55 \text{ m}^3 \text{ s}^{-1}$ , while subsequent forecast updates produce estimates in the range of  $60\text{--}80 \text{ m}^3 \text{ s}^{-1}$ . Peak timing varies by roughly one day across forecast cycles, with deviations primarily attributable to timing and intensity errors in the underlying IFS precipitation forecasts at short lead times. Despite these uncertainties, the event is robustly detected well in advance, demonstrating how the model’s conservative event-detection strategy translates into reliable early warning for high-impact floods.

### 4.3 Benchmarking: AIFL vs. Google Global Model

The AIFL model is benchmarked against the Google global flood model [20] using publicly released outputs archived on Zenodo [42]. The Google model is trained on 5,680 gauging stations, primarily from the GRDC, and employs a multi-source precipitation forcing pipeline that combines ERA5-Land and IFS reanalyses with NOAA CPC gauge data and NASA IMERG satellite estimates [20]. The evaluation considers the 1,218 stations shared between both datasets over the test period 2021–2024.

Across this evaluation set, the Google model achieves slightly higher median skill than AIFL, with  $\text{KGE}'$  values of 0.678 versus 0.636, NSE of 0.624 versus 0.518, and Pearson correlation of 0.857 versus 0.808 (Figure 10). Bias ( $\beta$ ) and variability ( $\gamma$ ) ratios are close to 1.0 for both models, indicating comparable large-scale water balance and variability characteristics. At the station level, AIFL outperforms Google at 523 locations (42.9%), whereas Google is superior at 695 stations (57.1%). Performance differences are most pronounced at the extremes. A subset of 125 stations (10.3% of the shared set) exhibits very poor AIFL performance ( $\text{KGE}' < 0$ ). Of these, 44 stations (35%) are also poorly predicted by Google, indicating that many failures occur in inherently challenging basins with complex hydrology or with systematically biased forcing data. In the remaining cases where AIFL skill is low, the Google model demonstrates moderate to high predictive skill. This divergence highlights specific instances where the Google model’s multi-source forcing or architectural features successfully mitigate failure modes encountered by the more streamlined AIFL model. The evaluation set spans a broad range of hydrological scales,

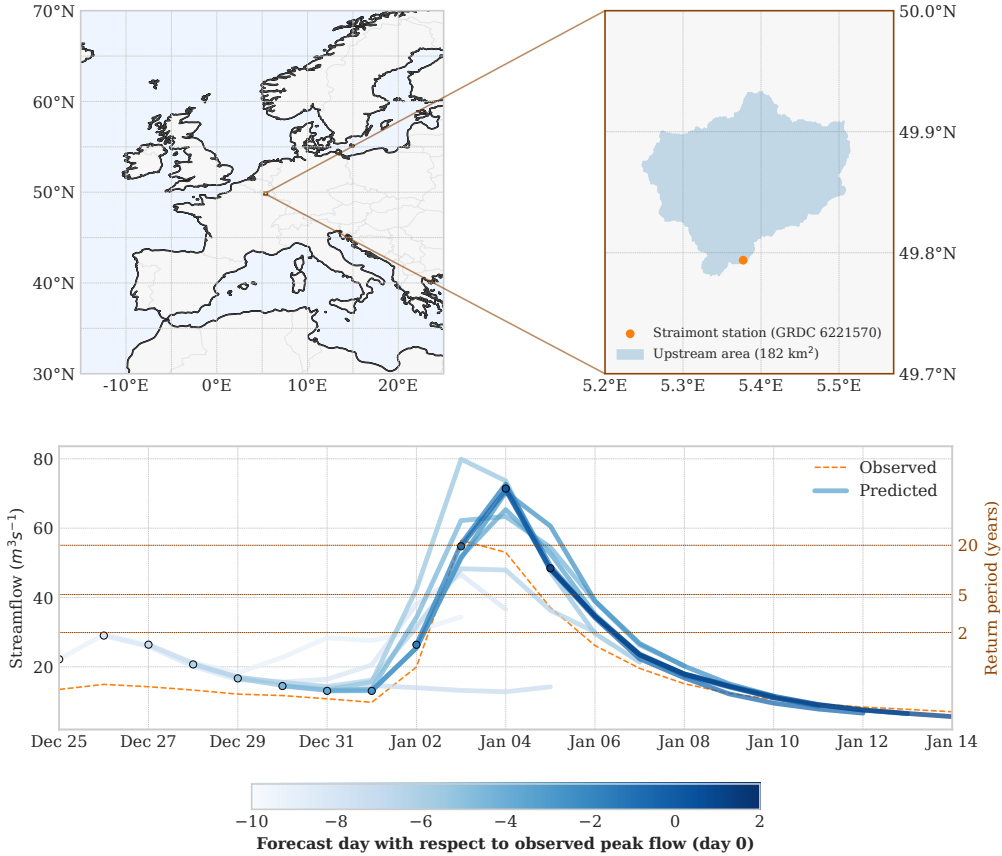


Figure 8: Flood event case study for Storm Henk (January 2024) at the Straimont station in Belgium, which drains a  $182 \text{ km}^2$  catchment (GRDC ID 6221570). Top: station location and upstream catchment. Bottom: observed streamflow (orange dashed) and AIFL forecasts (blue shades; darker colors indicate shorter lead times), shown relative to return-period thresholds indicated on the y-axis.

from headwater catchments under  $1,000 \text{ km}^2$  to large continental basins (Figure 9A). Performance systematically varies with basin size: in smaller catchments, AIFL is highly competitive, outperforming Google at 55% of stations, reflecting its capacity to capture rapid hydrological responses. For larger basins, the fraction of stations where AIFL underperforms rises to 62%. Beyond median skill, AIFL demonstrates consistent performance across all basin sizes, providing a stable global baseline. While the Google model achieves slightly higher maximum skill in large basins, its performance exhibits greater variability in smaller catchments, with a wider interquartile range (IQR = 0.504), whereas AIFL maintains relatively stable skill across all basin sizes (IQR = 0.42) (Figure 9B). Spatial patterns of performance differences (Figure 9C) do not indicate strong geographic clustering, though modest regional gains are observed in Australia and Northern Europe, offset by Google’s advantages in parts of North America and Southern Africa.

The observed performance gap relative to Google can be attributed to two main factors. First, the multi-source precipitation forcing employed by Google enables the network to exploit complementary error structures across reanalysis, gauge-based, and satellite-derived products, reducing extreme failures in data-sparse or meteorologically complex regions. Second, the Google model utilises a distributional training objective based on an asymmetric Laplace loss [20]. This choice enables the model to represent a conditional distribution of discharge, providing inherent probabilistic calibration and increased robustness to outliers. In contrast, AIFL relies on a deterministic loss function with a simpler forcing pipeline. Despite these differences, AIFL

achieves competitive median skill at most stations and matches or exceeds Google at over 40% of locations, offering a transparent, reproducible, and operationally streamlined global baseline suitable for research, diagnostic evaluation, and deployment where simplicity and reproducibility are priorities.

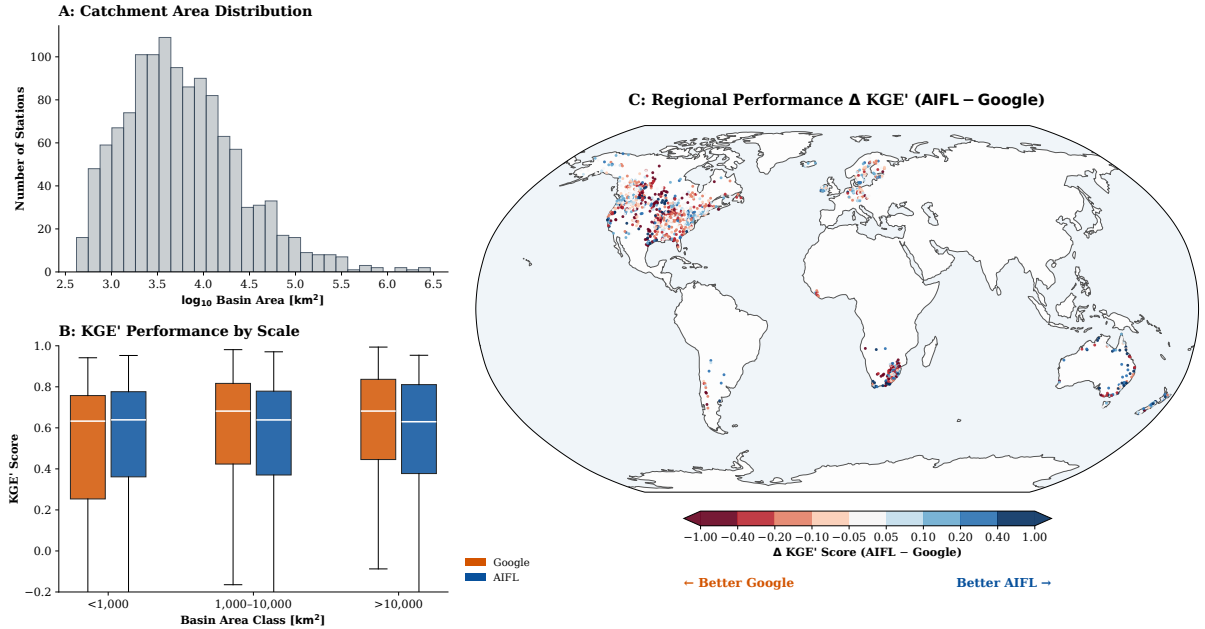


Figure 9: Diagnostic benchmarking of AIFL against the Google global model. (A) Distribution of catchment areas for the shared evaluation stations. (B) KGE' performance stratified by basin area class ( $<1,000 \text{ km}^2$ ,  $1,000\text{--}10,000 \text{ km}^2$ ,  $>10,000 \text{ km}^2$ ), showing medians and interquartile ranges for both models. (C) Spatial distribution of KGE' differences (AIFL minus Google); blue markers indicate regions where AIFL achieves higher skill, red markers indicate basins where Google performs better.

## 5 Conclusion and Future Directions

This study presents AIFL, a machine learning model for global streamflow forecasting, designed to provide robust predictions under operational forcing conditions. The model is trained end-to-end using the CARAVAN ecosystem, employing a two-stage strategy that first pretrains on four decades of ERA5-Land reanalysis and subsequently finetunes on operational IFS control forecasts. This approach enables adaptation to the statistical properties and biases of near-real-time forecast inputs, yielding median KGE' of 0.66, NSE of 0.53 and near-perfect volume conservation with a median bias ratio ( $\beta$ ) of 1.00, over the 2021–2024 test period at 2,003 gauged basins.

When evaluated against the Google global flood model at 1,218 shared stations, AIFL matches or exceeds Google skill at 42.9% of locations. Differences are most pronounced at extremes: a subset of stations exhibits poor performance for AIFL but moderate-to-high skill for Google, highlighting basins where model-specific factors—rather than universally challenging conditions—drive errors. Performance varies systematically with basin size, with AIFL performing better in smaller catchments, while Google has an advantage in the largest basins. Beyond median skill, AIFL provides stable and consistent predictions across all basin sizes, whereas Google shows increased variability in smaller catchments.

Event-based verification indicates that AIFL operates with a highly conservative detection profile. Under a strict zero-day timing criterion, the model achieves a global precision of 1.0,

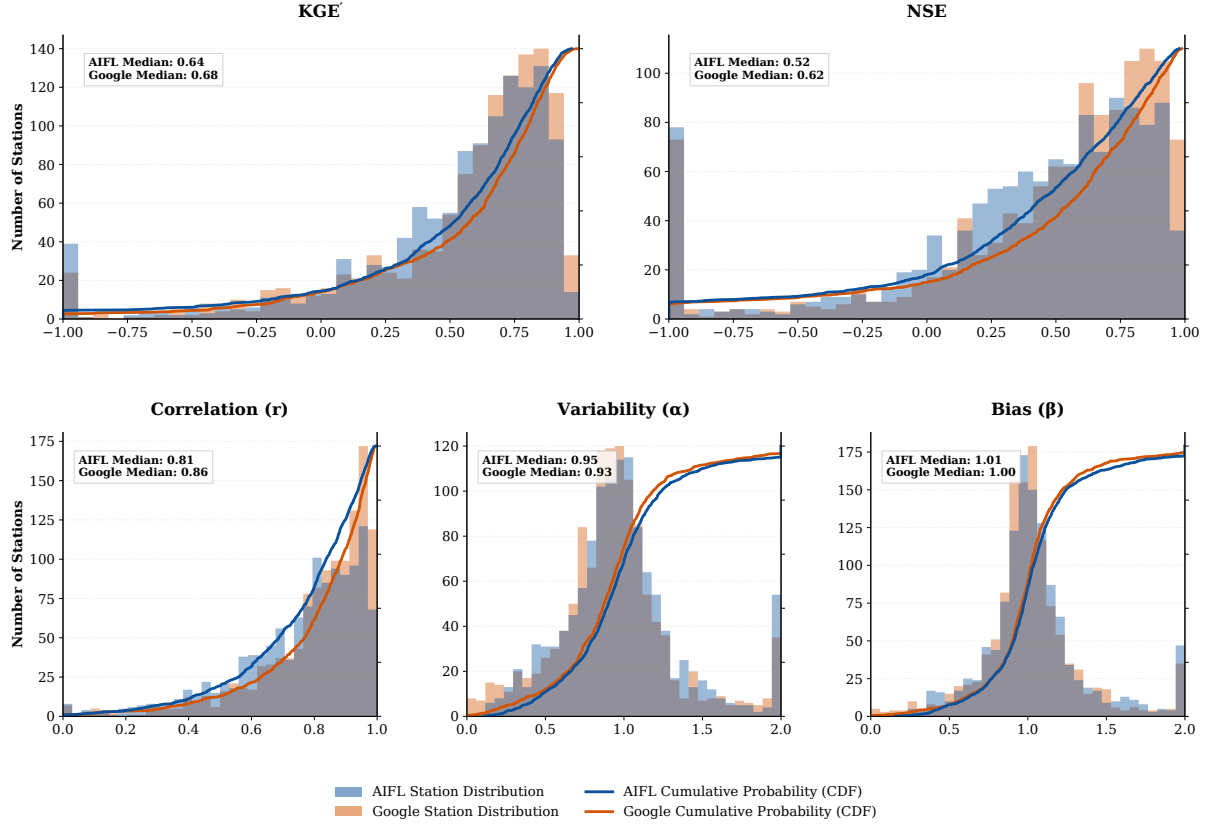


Figure 10: Comparative performance metrics between AIFL (navy) and the Google global model (orange) across 1,218 shared stations. Histograms show the frequency of performance scores, while curves show empirical cumulative distribution functions (ECDFs) for KGE', NSE, correlation, variability, and bias.

effectively eliminating false alarms for return periods ranging from 1.5 to 50 years. While recall remains limited—capturing approximately half of frequent events and a third of extreme 50-year floods—this behaviour prioritizes high-confidence alerts, a critical feature for maintaining user trust in operational early-warning contexts. The practical utility of this strategy was evidenced during the January 2024 Storm Henk floods in Belgium, where AIFL successfully identified a 20-year flood signal six days in advance.

Several avenues remain for future development. While this study utilised a deterministic loss function, future iterations could transition toward distributional objectives to enable inherent uncertainty quantification. Moreover, the integration of probabilistic ensemble forcing could further refine event detection and support risk-based decision-making. Future research may also investigate the impact of multi-source precipitation products on improving recall for rare extremes. By providing a transparent and reproducible architecture that balances consistency with competitive skill, AIFL establishes a transparent, reproducible, and operationally viable baseline for global streamflow forecasting.

## Code and Data Availability

The model code and weights are intended to be hosted at <https://huggingface.co/ecmwf> as part of a broader release of Earth system model components; however, at the time of this preprint, the repository is still under preparation and not yet publicly accessible. The CARAVAN and MultiMet datasets remain available via Zenodo and Google Cloud Storage as described in the original publications.

## Author Contributions

Following the CRediT taxonomy: **Maria Luisa Taccari**: Conceptualization, Methodology, Software, Formal analysis, Investigation, Writing – original draft. **Kenza Tazi**: Case study design and analysis, Investigation, Writing – review & editing. **Oisín M. Morrison**: Data curation, Validation. **Andreas Grafberger**: Data curation, Validation. **Juan Colonese**: Model operationalization, Software. **Corentin Carton de Wiart**: Model operationalization, Software. **Christel Prudhomme**: Project shaping, Supervision, Writing – review. **Cinzia Mazzetti**: Project shaping. **Matthew Chantry**: Project shaping, Funding acquisition. **Florian Pappenberger**: Project shaping, Funding acquisition. All authors have read and agreed to the final version of the manuscript.

## Acknowledgments

The authors would like to thank Grey Nearing and Alden Keefe Sampson for the fruitful discussions that helped shape this work. The work presented in this paper has been produced in the context of the European Union’s Destination Earth Initiative and relates to tasks entrusted by the European Union to the European Centre for Medium-Range Weather Forecasts implementing part of this Initiative with funding by the European Union. Views and opinions expressed are those of the author(s) only and do not necessarily reflect those of the European Union or the European Commission. Neither the European Union nor the European Commission can be held responsible for them.

## References

- [1] L. Alfieri et al. GloFAS—global ensemble streamflow forecasting and flood early warning. *Hydrology and Earth System Sciences*, 17(3):1161–1175, 2013.
- [2] V. P. Singh. *Hydrologic Modeling: Progress and Future Directions*. MDPI, 2018.
- [3] C. Prudhomme et al. Global hydrological reanalyses: The value of river discharge information for world-wide downstream applications – the example of the global flood awareness system GloFAS. *Meteorological Applications*, 31(2):e2192, 2024.
- [4] S. Grimaldi et al. GloFAS v4.0: Towards hyper-resolution hydrological modelling at the global scale. *Copernicus Meetings*, EGU23-15711, 2023.
- [5] S. Lang et al. Aifs: Ecmwf’s data-driven forecasting system, 2024. arXiv preprint.
- [6] G. Moldovan et al. An update to ecmwf’s machine-learned weather forecast model aifs, 2025. arXiv preprint.
- [7] Louise Slater, Georgios Blougouras, Liangkun Deng, Qimin Deng, Emma Ford, Anne Hoek van Dijke, Feini Huang, Shijie Jiang, Yinxue Liu, Simon Moulds, Andrew Schepen, Jiabo Yin, and Boen Zhang. Challenges and opportunities of ml and explainable ai in large-sample hydrology. *Philosophical Transactions of the Royal Society A: Mathematical, Physical and Engineering Sciences*, 383(2302), 7 2025.
- [8] F. Kratzert, M. Gauch, D. Klotz, and G. Nearing. Hess opinions: Never train a long short-term memory (lstm) network on a single basin. *Hydrology and Earth System Sciences*, 28(17):4187–4201, 2024.

- [9] F. Kratzert, D. Klotz, C. Brenner, G. Klambauer, and S. Hochreiter. Toward learning universal, regional, and local hydrological behaviors via machine learning applied to large-sample datasets. *Water Resources Research*, 55(2):1392–1411, 2019.
- [10] K. Ruparell et al. Hydra-lstm: A semi-shared machine learning architecture for prediction across watersheds. *Artificial Intelligence for the Earth Systems*, 4(3):240103, 2025.
- [11] Y. Wang, L. Zhang, N. B. Erichson, and T. Yang. Investigating the streamflow simulation capability of a new mass-conserving long short-term memory (mc-lstm) model across the contiguous united states. *Journal of Hydrology*, 658:133161, 2025.
- [12] G. Nearing et al. What role does hydrological science play in the age of machine learning? *Water Resources Research*, 57(3):e2020WR028091, 2021.
- [13] F. Scholz, M. Traub, C. Zarfl, T. Scholten, and M. V. Butz. Fully differentiable, fully distributed rainfall-runoff modeling. *EGUsphere*, pages 1–37, 2025.
- [14] Z. Moshe et al. Hydroneets: Leveraging river structure for hydrologic modeling, 2020. arXiv preprint.
- [15] M. H. Shams Eddin, Y. Zhang, S. Kollet, and J. Gall. Rivermamba: A state space model for global river discharge and flood forecasting, 2025. arXiv preprint.
- [16] Y. Yang et al. Combining grid-level lstm runoff with the rapid routing engine, 2025.
- [17] T. Bindas et al. Improving river routing using a differentiable muskingum–cunge model and physics-informed machine learning. *Water Resources Research*, 60(1):e2023WR035337, 2024.
- [18] B. Kraft et al. Ch-run: A deep-learning-based spatially contiguous runoff reconstruction for switzerland. *Hydrology and Earth System Sciences*, 29(4):1061–1082, 2025.
- [19] B. Kraft, M. Kauzlaric, W. H. Aeberhard, M. Zappa, and L. Gudmundsson. Drop: A scalable deep learning approach for runoff simulation and river routing. *Authorea Preprints*, 2025.
- [20] G. Nearing et al. Global prediction of extreme floods in ungauged watersheds. *Nature*, 627:559–563, 2024.
- [21] A. J. Newman et al. Development of a large-sample watershed-scale hydrometeorological data set for the contiguous usa. *Hydrology and Earth System Sciences*, 19(1):209–231, 2015.
- [22] F. Kratzert et al. Caravan – a global community dataset for large-sample hydrology. *Scientific Data*, 10(13), 2023.
- [23] Yihan Wang, Annan Yu, Lujun Zhang, Charuleka Varadharajan, and N Benjamin Erichson. Hydrodiffusion: Diffusion-based probabilistic streamflow forecasting with a state space backbone. *arXiv preprint arXiv:2512.12183*, 2025.
- [24] Oliver Konold, Moritz Feigl, Patrick Podest, Christoph Klingler, and Karsten Schulz. Bi-ascast: Learning and adjusting real time biases from meteorological forecasts to enhance runoff predictions. *EGUsphere*, pages 1–25, 2025.
- [25] G. Shalev and F. Kratzert. Caravan multimet: Extending caravan with multiple weather nowcasts and forecasts, 2025. arXiv preprint.

- [26] A. Ryd and G. S. Nearing. Fine flood forecasts: Incorporating local data into global models through fine-tuning. In *ICLR 2025 Workshop on Tackling Climate Change with Machine Learning*, 2025.
- [27] Richard Arsenault, François Brissette, Jean-Luc Martel, Magali Troin, Guillaume Lévesque, Jonathan Davidson-Chaput, Musandji Fuamba, David Huard, and Annie Poulin. A comprehensive, multisource database for hydrometeorological modeling of 14,425 north american watersheds. *Scientific Data*, 7(1):243, 2020.
- [28] Nereus Addor, Andrew J. Newman, Naoki Mizukami, and Martyn P. Clark. The CAMELS data set: catchment attributes and meteorology for large-sample studies. *Hydrology and Earth System Sciences*, 21(10):5293–5313, 2017.
- [29] C. Färber, H. Plessow, S. A. Mischel, F. Kratzert, N. Addor, G. Shalev, and U. Loosser. GRDC-Caravan: extending Caravan with data from the Global Runoff Data Centre. *Earth System Science Data*, 17:4613–4625, 2025.
- [30] Hoshin V. Gupta, Harald Kling, Koray K. Yilmaz, and Guillermo F. Martinez. Decomposition of the mean squared error and NSE performance criteria: Implications for improving hydrological modelling. *Journal of Hydrology*, 377(1–2):80–91, 2009.
- [31] Thomas Haiden, Martin Janousek, Jean Bidlot, Laura Ferranti, F. Prates, Frédéric Vitart, Peter Bauer, and David Richardson. Evaluation of ECMWF forecasts, including the 2016 resolution upgrade. Technical Memorandum 792, ECMWF, 2016.
- [32] Simon Linke, Bernhard Lehner, Catherine Ouellet Dallaire, Joseph Ariwi, Günther Grill, Mira Anand, Peter Beames, Vicente Burchard-Levine, Shawna Maxwell, Heloisa Moidu, et al. Global hydro-environmental sub-basin and river reach characteristics at high spatial resolution. *Scientific Data*, 6(1):283, 2019.
- [33] Frederik Kratzert, Martin Gauch, Grey Nearing, and Daniel Klotz. Neuralhydrology — a python library for deep learning research in hydrology. *Journal of Open Source Software*, 7(71):4050, 2022.
- [34] F. Kratzert et al. Towards learning universal, regional, and local hydrological behaviors via machine learning applied to large-sample datasets. *Hydrology and Earth System Sciences*, 23(12):5089–5110, 2019.
- [35] Joaquín Muñoz-Sabater, Emanuel Dutra, Anna Agustí-Panareda, Clément Albergel, Gabriele Arduini, Gianpaolo Balsamo, Souhail Boussetta, Margarita Choulga, Shaun Harrigan, Hans Hersbach, Brecht Martens, Diego G. Miralles, María Piles, Nemesio J. Rodríguez-Fernández, Ervin Zsoter, Carlo Buontempo, and Jean-Noël Thépaut. ERA5-Land: a state-of-the-art global reanalysis dataset for land applications. *Earth System Science Data*, 13(9):4349–4383, 2021.
- [36] Harald Kling, Martin Fuchs, and Maria Paulin. Runoff conditions in the upper Danube basin under an ensemble of climate change scenarios. *Journal of Hydrology*, 424–425:264–277, 2012.
- [37] Wouter J M Knoben, Jim E Freer, and Ross A Woods. Inherent benchmark or not? Comparing Nash–Sutcliffe and Kling–Gupta efficiency scores. *Hydrology and Earth System Sciences*, 23(10):4323–4331, 2019.
- [38] Stefania Grimaldi and Karen O'Regan. GloFAS v4 calibration hydrological model performance. Copernicus Emergency Management Service (CEMS) Wiki, 2023. Accessed: 2025-01-25.

- [39] Daniel N Moriasi, Jeffrey G Arnold, Michael W Van Liew, Ronald L Bingner, R Darren Harmel, and Tamie L Veith. Model evaluation guidelines for systematic quantification of accuracy in watershed simulations. *Transactions of the ASABE*, 50(3):885–900, 2007.
- [40] Lindsey R. Barnes, Eve C. Gruntfest, Mary H. Hayden, David M. Rogers, and Kevin W. Schulz. False alarms and close calls: A conceptual model of warning trust. *Weather and Forecasting*, 22(5):1140–1147, 2007.
- [41] Kai Schröter, Tobias Sieg, Kristin Vogel, Jacek Vogel, Maite Iturriza, Alberto Arzelus, Jon Urrutia, Joseba Zubieta, Maider Garmendia, Matthias Kemter, et al. Effectiveness and efficiency of public flood preparedness and emergency response. *Hydrology and Earth System Sciences*, 21(4):2001–2017, 2017.
- [42] Grey Nearing. Global prediction of extreme floods in ungauged watersheds, 2023. Zenodo, Version 3. DOI: 10.5281/zenodo.10397664.